Science and Technology Indonesia
e-ISSN:2580-4391 *p*-ISSN:2580-4405
Vol. 10, No. 3, July 2025

Research Paper

Amine-Functionalized Mesoporous Silica SBA-15 for Enhanced Solubility and Release Rate of Gliclazide

Fasqina Sayyidina[1], Azhoma Gumala[2], Erizal Zaini[2], Dini Hanifa[3], Uswatul Hasanah[2*]

[1]*Undergraduate Programme of Pharmacy, Faculty of Pharmacy, Universitas Andalas, Padang, West Sumatera, 25163, Indonesia*
[2]*Department of Pharmaceutics, Faculty of Pharmacy, Universitas Andalas, Padang, West Sumatera, 25163, Indonesia*
[3]*Department of Pharmaceutical Chemistry, Faculty of Pharmacy, Universitas Andalas, Padang, West Sumatera, 25163, Indonesia*
*__Corresponding author__: uswatulhasanah@phar.unand.ac.id

Abstract
Gliclazide (GLI), a sulfonylurea-class antidiabetic drug, exhibits poor aqueous solubility, limiting its bioavailability. This study aimed to enhance gliclazide's solubility and dissolution rate by adsorbing it into mesoporous silica SBA-15 and amine-functionalized SBA-15 (SBA-15-A). SBA-15 was synthesized using Pluronic® P123 as a template and tetraethyl orthosilicate (TEOS) as the silica precursor, while 3-aminopropyltriethoxysilane (APTES) was used to introduce amine functional groups. Gliclazide was loaded into SBA-15 and SBA-15-A at a 1:3 mass ratio. The materials (GLI, SBA-15, SBA-15-A, GLI-SBA, and GLI-SBA-A) were characterized using nitrogen adsorption-desorption isotherms, differential scanning calorimetry (DSC), Fourier-transform infrared spectroscopy (FT-IR), scanning electron microscopy (SEM), transmission electron microscopy (TEM), and powder X-ray diffraction (PXRD). Characterization revealed that the pore diameters of SBA-15 and SBA-15-A were 6.079 nm and 5.483 nm, respectively. FT-IR confirmed the interaction between gliclazide and the mesoporous carriers. SEM and TEM analysis showed crystalline gliclazide and rod-shaped morphologies for the mesopores samples. DSC and PXRD results indicated that most of the gliclazide had been converted to an amorphous form. Solubility testing over 24 hours showed that GLI-SBA and GLI-SBA-A improved gliclazide solubility by 1.375- and 2.334-fold, respectively, compared to pure gliclazide. Dissolution testing in distilled water revealed a 6.033-fold and 3.887-fold increase in the release rate at 5 minutes for GLI-SBA and GLI-SBA-A, respectively. Both solubility and release rate improvements were statistically significant ($p < 0.05$). These findings suggest that amine functionalization of SBA-15 effectively enhances the solubility and dissolution rate of gliclazide.

Keywords
Gliclazide, SBA-15, APTES (3-Aminopropyltriethoxysilane), Solubility, Release Rate

Received: 14 March 2025, Accepted: 8 June 2025
https://doi.org/10.26554/sti.2025.10.3.963-971

1. INTRODUCTION

Noninsulin-dependent diabetic mellitus (NIDDM) is a chronic disease that requires long-term treatment (Banday et al., 2020). Using medications with a frequency of more than once a day reduces patient compliance (Weeda et al., 2016). Therefore, a controlled drug delivery system is needed to improve patient compliance (Simos et al., 2021). Controlled delivery refers to controlling the rate of drug release into the body. With this method, we can maintain the release profile and the amount of drug released, allowing patients to take the medication less frequently (Domingo-Lopez et al., 2022; Wang and Duan, 2019). Controlled delivery systems are also designed to maintain consistent drug levels in the bloodstream throughout the day.

Gliclazide (GLI), one of the drugs used to treat this disease, works by activating pancreatic β-cells to release insulin, thereby increasing insulin secretion (Sahin et al., 2024). Typically, this medication needs to be taken more than once a day to maintain stable drug levels in the blood. Gliclazide is practically insoluble in water (55 mg/L at 37°C), which results in low bioavailability of only about 59% (Bindal et al., 2024; Maggi et al., 2015). This issue can be addressed through various methods, such as increasing the solubility of the active compound. Mesoporous silica is an example of a modification currently being extensively studied. With mesoporous silica, the drug dissolves gradually, becoming more effective (He et al., 2017; Knapik-Kowalczuk et al., 2020; Zhang et al., 2024).

Based on previous research, mesoporous silica materials such as Santa Barbara Amorphous-15 (SBA-15) have been proven to increase the solubility of curcumin by 2.201 fold and usnic acid by 5.15 fold (Fitriani et al., 2023, 2024). Meanwhile,

SBA-15 functionalized with amino groups can increase the solubility of sulindac by 5.333 fold (Dadej et al., 2021). The most commonly used functionalization is the addition of amino groups ($-NH_2$) (Estevão et al., 2021). These groups may modify the interaction between gliclazide and mesoporous SBA-15, allowing for more controlled and stable drug release than conventional sustained-release formulations.

While extensive research has been conducted on the interactions of amoxicillin, ibuprofen, and sulindac with SBA-15 and amine-functionalized SBA-15, gliclazide's unique structural and chemical characteristics require focused investigation. Amoxicillin, being zwitterionic and possessing multiple ionic groups, forms strong electrostatic interactions with amine-functionalized silica, thereby achieving significant drug loading and sustained release via ionic crosslinking (Yaghobi et al., 2019). On the other hand, ibuprofen acts as a weak acid with predominantly carboxylate groups, demonstrating moderate hydrogen bonding and weaker ionic interactions, leading to quicker release profiles from functionalized SBA-15 (Izquierdo-Barba et al., 2009). Similarly, sulindac, a nonsteroidal anti-inflammatory drug (NSAID) structurally akin to ibuprofen but featuring extra sulfonyl functional groups, has revealed enhanced solubility and controlled release when incorporated into amino-functionalized SBA-15, mainly due to improved hydrogen bonding and electrostatic interactions between the sulfonyl and amine groups (Dadej et al., 2021). In contrast, gliclazide differs from these medications as it includes sulfonylurea and amide groups, which encourage hydrogen bonding over strong ionic interactions and exhibit moderate polarity with limited ionization. Consequently, gliclazide's adsorption and release characteristics are anticipated to vary significantly, particularly concerning amine surface functionalization; thus, research is required. This research aims to study gliclazide's interaction with unfunctionalized and amine-functionalized SBA-15, offering vital insights for refining its controlled delivery system.

2. EXPERIMENTAL SECTION

2.1 Materials

Gliclazide was obtained from Tokyo Chemical Industry (Japan). Pluronic®P123 and sodium chloride were purchased from Sigma-Aldrich (USA). Tetraethyl orthosilicate (TEOS) was obtained by Tokyo Chemical Industry (Japan). Hydrochloric acid and pro-analytical grade ethanol were purchased from Merck (Germany). Anhydrous alcohol and 3-aminopropyltriethoxysil ane (APTES) were obtained from Sigma-Aldrich (USA).

2.2 Methods

2.2.1 Synthesis of SBA-15

SBA-15 was synthesized using Pluronic® P123 as a structure-directing agent and tetraethyl orthosilicate (TEOS) as the silica source. The synthesis followed a molar ratio of 1 TEOS: 0.02 P123: 6 HCl: 166 H_2O: 0.7 NaCl. Pluronic® P123 and NaCl were dissolved in a 2.0 M hydrochloric acid solution under constant stirring at 300 rpm and 25°C for 24 hours using a magnetic stirrer (Cimarec +, USA). Subsequently, TEOS was added dropwise to the solution, followed by stirring at 700 rpm and 25°C for 3 hours to allow hydrolysis and condensation. The mixture was then aged in an oven (Memmert UN 110, Germany) at 80°C for 24 hours to promote mesostructure development. The resulting white precipitate was collected by filtration, washed thoroughly with distilled water, and dried at 50°C for 14 hours. Finally, the dried solid was calcined in a furnace (Carbolite Gero CWF 1100, UK) at 550°C for 4 hours to remove the organic template, yielding pure mesoporous SBA-15 (Hasanah et al., 2021).

2.2.2 Functionalization of SBA-15 with Amines Group

Functionalization of SBA-15 was performed by refluxing 2.0 g of 3-aminopropyltriethoxysilane (APTES) with 2.0 g of SBA-15 in 60 mL of anhydrous ethanol at 78°C for 24 hours using a reflux apparatus. After the reaction, the resulting solid was separated by filtration and washed thoroughly with ethanol to remove unreacted APTES. The product was then dried in an oven (Memmert UN 110, Germany) at 60°C for 3 hours to yield amine-functionalized SBA-15 (SBA-15-A) (Liou et al., 2022).

2.2.3 Adsorption of Gliclazide on SBA-15 and SBA-15-A

A gliclazide solution with a concentration of 5 mg/mL was prepared by dissolving gliclazide in ethanol under continuous stirring at 300 rpm and 50 °C using a magnetic stirrer. Subsequently, SBA-15 or amine-functionalized SBA-15 (SBA-15-A) was added to the solution in three different drug-to-carrier weight ratios: 1:1, 1:2, and 1:3. The mixture was stirred continuously until the solvent fully evaporated. The resulting solids were collected, rinsed with 1 mL of ethanol to remove unadsorbed drug, and left to dry at room temperature, yielding GLI-SBA and GLI-SBA-A powders for each ratio. Differential scanning calorimetry (DSC) was then used to assess the degree of drug amorphization in each formulation, and the ratio exhibiting the greatest amorphous transformation was selected for further analysis. The amount of adsorbed gliclazide was determined by dissolving the loaded drug from the carrier in ethanol and quantifying it using UV-Vis spectrophotometry at 225 nm to calculate the adsorption efficiency.

Table 1. Gliclazide Adsorption Efficiency on SBA-15 and SBA-15-A

Sample	Average of Adsorption Efficiency (%) ± SD
GLI-SBA	99.4485 ± 0.8903
GLI-SBA-A	99.8570 ± 0.8170

2.2.4 Characterization of GLI, SBA-15, SBA-15-A, GLI-SBA, and GLI-SBA-A

The mesoporous silica sample's pore structure and surface area were analyzed using nitrogen adsorption-desorption isotherms

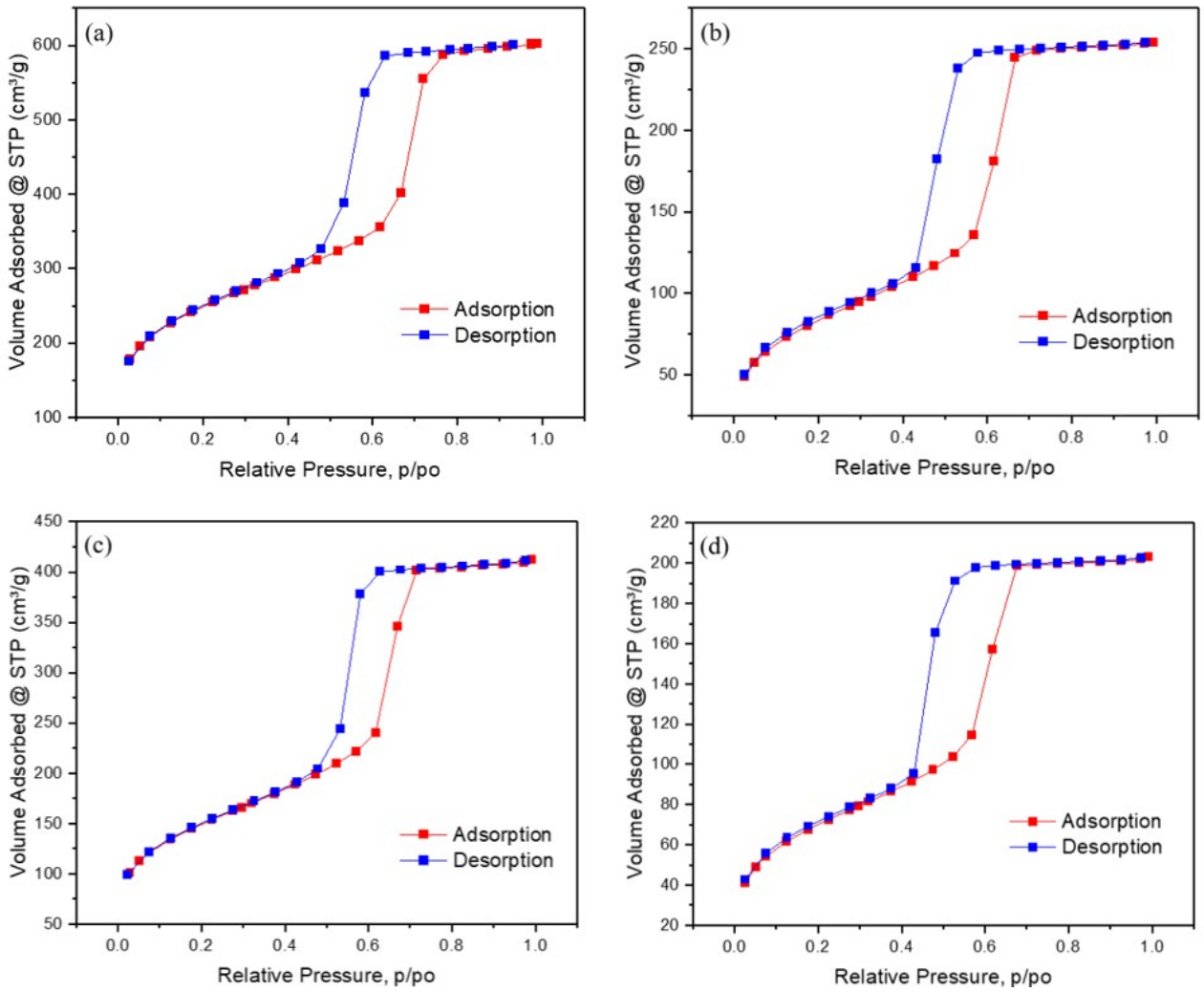

Figure 1. Nitrogen Adsorption-Desorption Isotherms of (a) SBA-15, (b) SBA-15-A, (c) GLI–SBA, and (d) GLI–SBA-A

Table 2. Pore Characteristics from Nitrogen Adsorption–Desorption Analysis

Parameters	SBA-15	SBA-15-A	GLI-SBA	GLI-SBA-A
Surface area (m^2/g)	878.254	280.438	489.108	229.786
Pore volume (cm^3/g)	0.899	0.378	0.615	0.302
Pore diameter (nm)	6.079	5.483	6.079	5.086

with a BET surface area and pore size analyzer (Quantachrome NovaTouch LX-4, USA). Thermal behavior was assessed by differential scanning calorimetry (DSC) using a Shimadzu DSC-60 Plus instrument (Japan). Functional groups were identified using Fourier-transform infrared (FT-IR) spectroscopy (Shimadzu IRTracer-100 AH, Japan). Surface morphology was observed using scanning electron microscopy (SEM; JEOL JSM 6510 LA, Japan), while the internal structure was examined using transmission electron microscopy (TEM; Hitachi HR-TEM H9500, Japan). Pow X-ray diffraction (PXRD) evaluated crystalline and amorphous phases using a PANalytical X'Pert Pro diffractometer (Model MPD PW3040/60, The Netherlands).

2.2.5 Solubility Test

The solubility of intact gliclazide (GLI), GLI-SBA, and GLI-SBA-A powders were evaluated in distilled water by shaking the samples in an orbital shaker (Memmert WNB 22, Germany) at 25°C for 24 hours. After equilibration, the suspensions were filtered, and the concentration of gliclazide in the filtrate was quantified using a UV-Vis spectrophotometer (Shimadzu UV-1700, Japan) at the drug's maximum absorption wavelength of 225 nm. Each experiment was performed in triplicate. Data were analyzed using one-way analysis of variance (ANOVA)

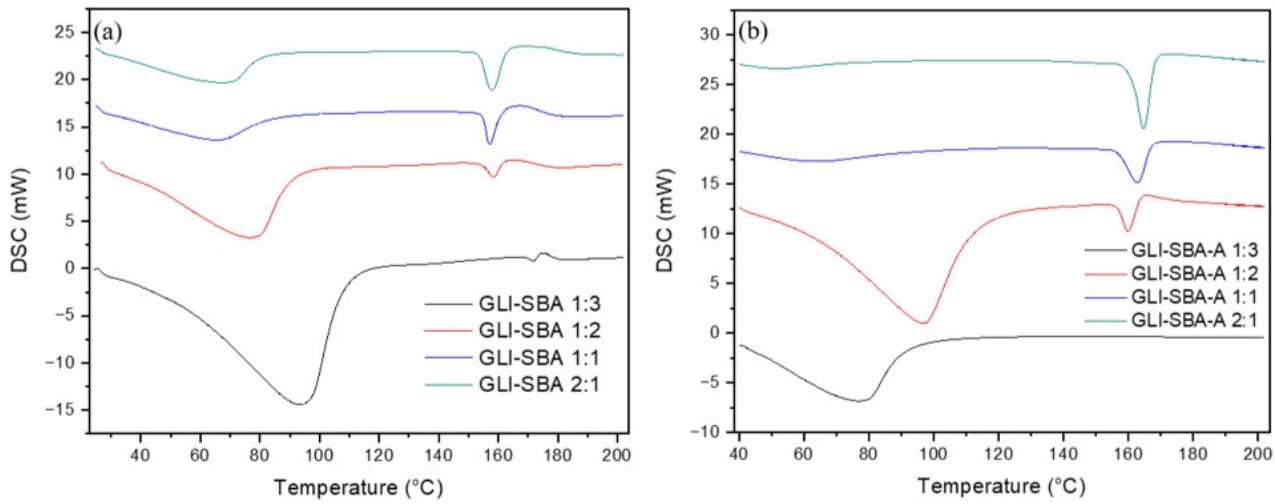

Figure 2. DSC Thermograms of (a) GLI–SBA and (b) GLI–SBA-A

Table 3. FTIR Analysis of Gliclazide, SBA-15, SBA-15-A, GLI–SBA, and GLI–SBA-A

Wavenumbers (cm^{-1})				
Gliclazide	SBA-15	SBA-15-A	GLI-SBA	GLI-SBA-A
3269.85 (N–H stretching)	3745.13 (O–H stretching)	2920.65 (C–H stretching)	2848.46 (C–H stretching)	2917.41 (C–H stretching)
2917.89 (C–H stretching)	3245.65 (O–H stretching)	1539.76 (C=O stretching)	1700.97 (C=O stretching)	1708.69 (C=O stretching)
1707.72 (C=O stretching)	2920.51 (C–H stretching)	1033.34 (Si–O–Si)	1597.32 (C=C stretching)	1596.35 (C=C stretching)
1595.87 (C=C stretching)	1624.17 (C=C stretching)	787.92 (C–N bending)	1539.46 (C=O stretching)	1538.49 (C=O stretching)
1431.94 (C–H bending)	1537.54 (C–O stretching)		1457.98 (C–H bending)	1457.98 (C–H bending)
1345.64 (S=O stretching)	1458.67 (C–H stretching)		1340.82 (S=O stretching)	1346.60 (S=O stretching)
1287.78 (C–N stretching)	1045.82 (Si–O–Si stretching)		1058.29 (Si–O–Si stretching)	1049.13 (Si–O–Si stretching)
666.79 (C–S stretching)	804.02 (Si–O–H bending)		798.41 (C–N bending)	792.15 (C–N bending)

with SPSS software to assess statistical significance.

2.2.6 Release Rate Test

The release profiles of GLI, GLI-SBA, and GLI-SBA-A powders were evaluated using a Type II dissolution apparatus (paddle type) (SR8 Plus Dissolution Test Station, Hanson, USA). An amount of powder equivalent to 30 mg of gliclazide was added to 900 mL of distilled water maintained at 37 ± 0.5 °C with a paddle rotation speed of 100 rpm. Samples of 5 mL were withdrawn at predetermined intervals (5, 10, 15, 30, 45, 60, 90, 150, 210, 330, 450, and 570 minutes) and immediately replaced with an equal volume of fresh distilled water to maintain the media volume. The concentration of gliclazide in the samples was determined using a UV-Vis spectrophotometer (Shimadzu UV-1700, Japan) at the drug's maximum absorbance wavelength of 225 nm. All experiments were performed in triplicate, and statistical analysis was conducted using one-way ANOVA in SPSS software to evaluate significant differences.

2.2.7 Physical Stability Test

The GLI-SBA and GLI-SBA-A samples were stored in a climatic chamber (Memmert HPPeco, Germany) at 40°C and 75% relative humidity for one month to assess their physical stability. After the storage period, physical stability was evaluated by powder X-ray diffraction (PXRD) analysis using a PANalytical X'Pert Pro diffractometer (Model MPD PW3040/60, The Netherlands).

Table 4. PXRD Data of Gliclazide, SBA-15, SBA-15-A, GLI–SBA, and GLI–SBA-A

	Intensity				
Pos 2θ (°)	Gliclazide	SBA-15	SBA-15-A	GLI–SBA	GLI–SBA-A
10.5407	11907.02	842.44	817.89	2135.47	1234.58
14.9957	3907.90	703.91	665.46	1147.89	1031.99
17.1077	6945.82	691.61	700.41	1559.87	1110.64
18.2297	12234.62	709.56	707.81	1629.82	1304.46
20.8367	7147.17	799.45	861.73	1323.51	1407.11

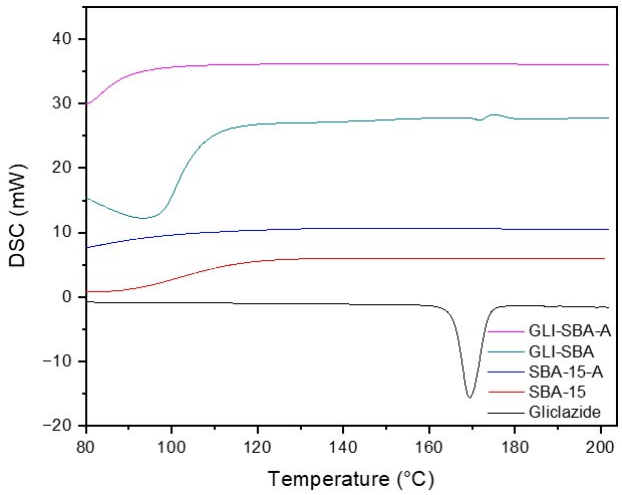

Figure 3. DSC Thermograms of Gliclazide, SBA-15, SBA-15-A, GLI–SBA, and GLI–SBA-A.

3. RESULTS AND DISCUSSION

Based on the characterization results using the nitrogen adsorption-desorption isotherm test, as shown in Figure 1, a hysteresis loop is observed at a relative pressure of 0.4 – 0.8, indicating the formation of a type IV isotherm curve. The type IV isotherm curve with a hysteresis loop is a characteristic of porous materials (Maleki and Hamidi, 2016).

In addition, characterization was performed for each ratio using thermal analysis with DSC, as shown in Figure 2. The thermogram indicates that in the GLI-SBA and GLI-SBA-A samples with a 1:3 ratio, almost no endothermic peak is observed, suggesting that gliclazide is well adsorbed into the mesopores of SBA-15-A. However, in the GLI-SBA sample with a 1:3 ratio, a slight endothermic peak is still visible, likely due to gliclazide adhering to the outer surface of the SBA-15 pores. According to the thermogram, it is evident that the adsorption of gliclazide into SBA-15 and SBA-15-A is effective at the 1:3 ratio.

To evaluate the adsorption efficiency of gliclazide into the mesopores of SBA-15/SBA-15-A, samples of GLI-SBA and GLI-SBA-A with a concentration of 12 μg/mL were used. The percentage of gliclazide adsorption efficiency in SBA-15 and SBA-15-A is presented in Table 1. Based on the table, the adsorption efficiency of gliclazide in the mesopores of SBA-15 and SBA-15-A was found to be 99.4485% and 99.8570%, respectively.

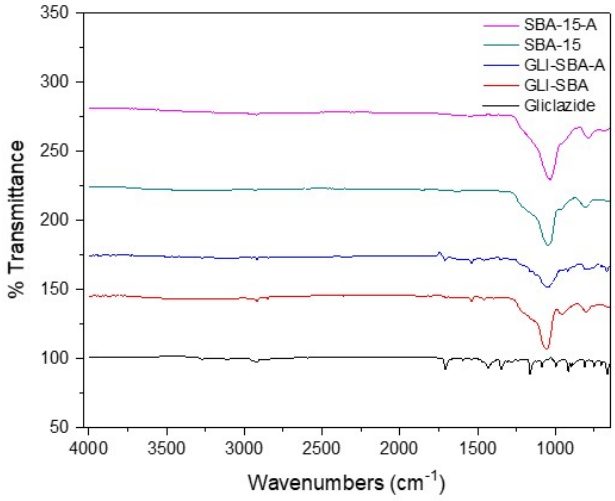

Figure 4. FTIR Spectra of Gliclazide, SBA-15, SBA-15-A, GLI–SBA, and GLI–SBA-A

After gliclazide is adsorbed into the mesopores, the hysteresis loop remains, indicating that the mesopores are still intact and not damaged during adsorption. Based on Table 2, the pore size of the mesoporous SBA-15 falls within the mesoporous size range of 2–50 nm. The characterization results also show that the pores of SBA-15 functionalized with amine groups exhibit a reduction in surface area, pore volume, and pore diameter, showing that adding amine groups to SBA-15 was successful. Furthermore, the pores of SBA-15 and SBA-15-A are well-filled with gliclazide. This is supported by the observation that the surface area and pore volume of SBA-15 and SBA-15-A loaded with gliclazide are smaller than SBA-15 and SBA-15-A without adsorption. The gliclazide entering SBA-15 and SBA-15-A fills the pores, reducing the surface area and pore volume. Meanwhile, the decrease in pore diameter is due to gliclazide adhering to the inner walls of the pores in SBA-15 and SBA-15-A.

The DSC thermal analysis results, as shown in Figure 3, indicate that gliclazide has an endothermic peak at 169°C. The endothermic peak signifies that gliclazide undergoes a phase transition at this temperature. The thermogram shows that gliclazide adsorption into SBA-15 and SBA-15-A is quite effec-

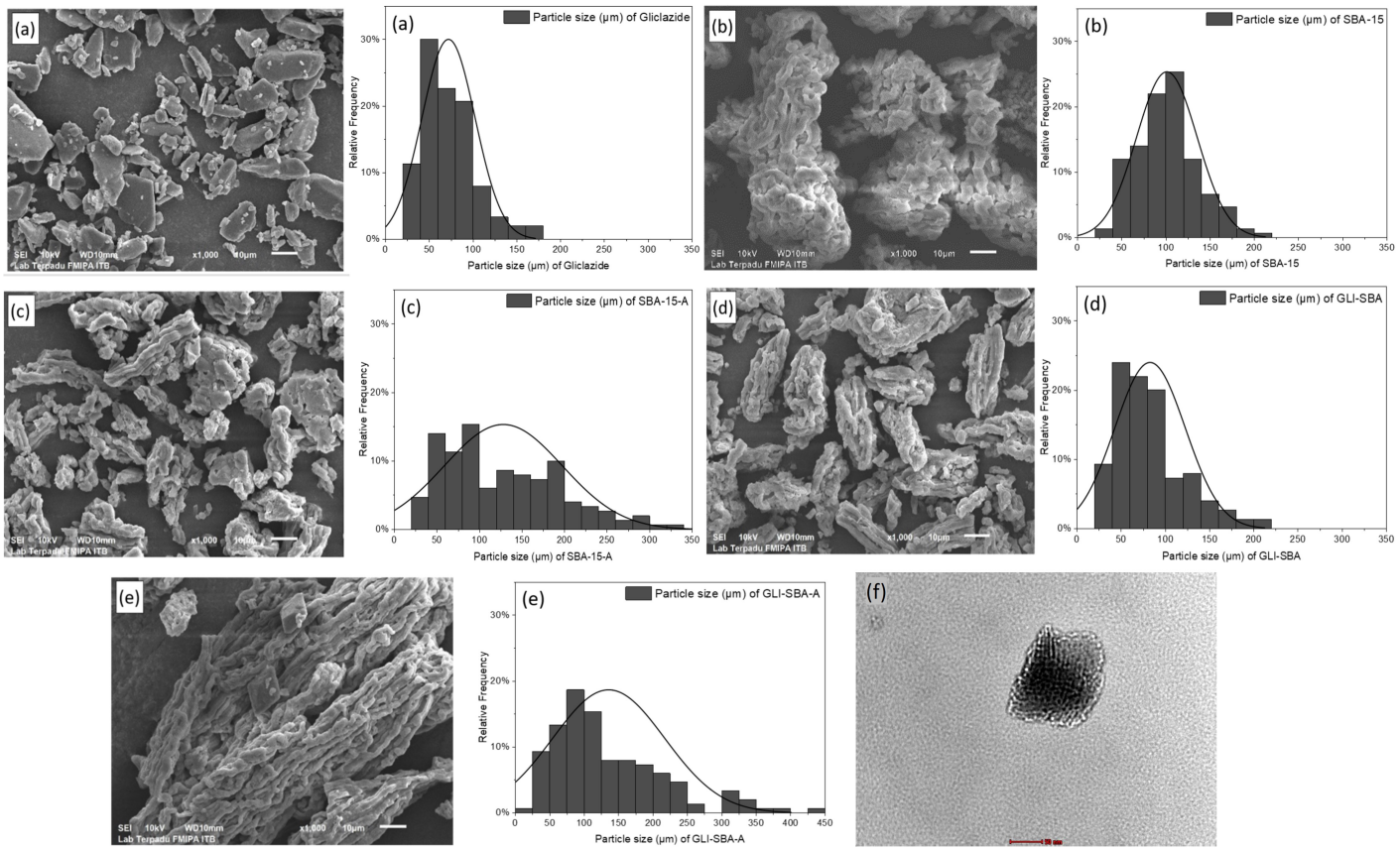

Figure 5. SEM Images and Particle Size Distribution of (a) Gliclazide, (b) SBA-15, (c) SBA-15-A, (d) GLI–SBA, (e) GLI–SBA-A; and (f) TEM Image of SBA-15

tive because almost no endothermic peaks are observed, consistent with studies conducted by Wawrzyńczak et al. (2023). Once adsorbed into SBA-15 and SBA-15-A, gliclazide finds it challenging to undergo crystal phase transitions due to the inhibition of crystallization, as gliclazide exists in an amorphous state within the mesopores of SBA-15 and SBA-15-A. The small and confined pore size restricts the active compound adsorbed within the SBA-15 and SBA-15-A pores from forming a crystal lattice (Budiman et al., 2024).

The results of the functional group analysis using FT-IR can be seen in Figure 4 and Table 3. The spectrum of SBA-15 functionalized with amine groups shows slight differences, namely the absence of O−H and H−O−H functional groups, indicating a reduction in hydroxyl and water content. A Si−O−Si stretching functional group is also observed at a wavenumber of 1033.34 cm^{-1}. Meanwhile, the wavenumber at 787.92 cm^{-1} indicates a C−N group's presence, signifying the amine group's successful functionalization. The spectrum also shows that the Si−O−Si stretching peak in the SBA-15-A sample is narrower and sharper compared to the SBA-15 sample, consistent with studies conducted by Liou et al. (2022) and Albayati et al. (2019). In the spectra of GLI-SBA and GLI-SBA-A, a combination of gliclazide and SBA-15/SBA-15-A spectra is observed. The chemical interactions between gliclazide and SBA-15 or SBA-15-A cause a slight shift in wavenumbers in the FTIR spectra. However, overall, no damage to the gliclazide structure is observed after its adsorption into SBA-15 and SBA-15-A.

Morphological analysis using scanning electron microscopy (Figure 5) shows that gliclazide crystals appear as aggregated particles. In contrast, SBA-15 and SBA-15-A exhibit rod-shaped morphological structures that tend to aggregate. This result is consistent with the previous study, which stated that the morphological structure of SBA-15 and SBA-15-A is rod-shaped (Liou et al., 2022). In addition, transmission electron microscopy analysis was also performed, as shown in Figure 5(f). SBA-15 sample displays a porous of material along the surface. This is aligned with the BET curves that show a pattern of a porous material. The morphology of GLI-SBA and GLI-SBA-A also shows similarities to the morphological structure of SBA-15 and SBA-15-A, indicating that gliclazide has been successfully adsorbed into the structure of SBA-15 and SBA-15-A.

The histogram of all samples (Figure 5) mostly fits the normal distribution but with right-skewed data. Particle size analysis revealed significant shifts in the modal particle sizes across the samples. Pure gliclazide and as-synthesized SBA-15 exhib-

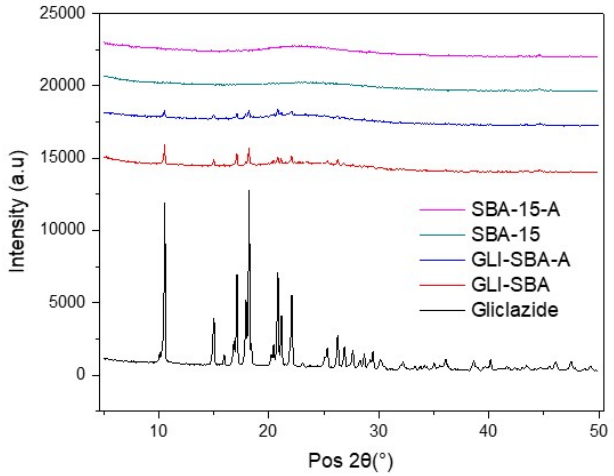

Figure 6. PXRD Patterns of Gliclazide, SBA-15, SBA-15-A, GLI–SBA, and GLI–SBA-A

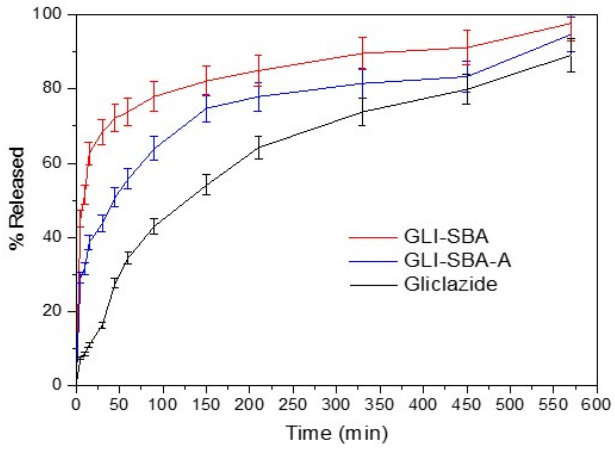

Figure 7. In Vitro Release Profiles of Gliclazide, GLI–SBA, and GLI–SBA-A in Distilled Water

ited micrometer-scale distributions, with modes at 40-60 µm and 100-120 µm, respectively. The amine-functionalized SBA-15 (SBA-15-A) showed a broader range with a mode at 80-100 µm, suggesting that the functionalization process might have induced some de-agglomeration of larger particles or subtle changes in their morphology (Munguía-Cortés et al., 2017). The incorporation of gliclazide into SBA-15 (GLI-SBA) caused its mode to align with pure gliclazide (40-60 µm), indicating that the drug loading process may have led to a more dispersed state of the composite by filling the pores. Most strikingly, the gliclazide-loaded amine-functionalized SBA-15 (GLI-SBA-A) displayed a distinct distribution ranging from 10-450 µm with a prominent mode at 80-100 µm. This shift suggests that the combined effect of amine functionalization and gliclazide loading effectively reduced the composite's dominant size to the lower micrometer range, presumably due to enhanced de-agglomeration or disruption of larger aggregates, with the drug molecules and amine groups potentially stabilizing these smaller structures through improved interactions (Pevná et al., 2023). The presence of some outliers observed above 300 µm in GLI-SBA-A indicates that while the majority of the material was efficiently reduced, a small fraction of larger macroscopic aggregates persisted.

Characterization using Powder X-ray diffraction (PXRD) aims to analyze the crystal phases in the sample. As shown in Figure 6, gliclazide exhibits diffraction peaks with high intensity, indicating that gliclazide is in crystalline form (Rajamma et al., 2015). In addition, no sharp diffraction peaks are observed for samples with amorphous properties such as SBA-15 and SBA-15-A. The specific diffraction peaks of crystalline gliclazide can be seen in Table 4, which are characteristic of its crystalline form. After gliclazide is adsorbed into SBA-15 and SBA-15-A, the diffractograms of GLI-SBA and GLI-SBA-A show no peak intensities similar to pure gliclazide. This analysis's results align with the research of Dadej et al. (2021). The diffraction patterns of GLI-SBA and GLI-SBA-A indicate that gliclazide has become amorphous.

According to the solubility test results in Table 5, the solubility of GLI-SBA and GLI-SBA-A increased in distilled water. The solubility of the GLI-SBA sample in distilled water increased by 1.375-fold compared to pure gliclazide. Meanwhile, the solubility of the GLI-SBA-A sample in distilled water increased by 2.334-fold compared to pure gliclazide. The enhanced solubility of gliclazide in SBA-15 and SBA-15-A is likely due to the inhibition of the recrystallization process of the active compound adsorbed within the mesoporous SBA-15 material. The mesopores of SBA-15 have tube/channel-like spaces whose thickness and rigidity prevent the active compound within from undergoing recrystallization (Letchmanan et al., 2017).

Table 5. Solubility of Gliclazide, GLI–SBA, and GLI–SBA-A in Distilled Water

Sample	Average gliclazide solubility ± SD (mg/L)	Solubility increase
Gliclazide	63.62 ± 0.253	-
GLI-SBA	87.5 ± 0.387	1.375-fold
GLI-SBA-A	148.515 ± 0.387	2.334-fold

Additionally, the reduction in particle size and the formation of hydrogen bonds via silanol groups on the surface of SBA-15 mesopores contribute to the increased solubility of GLI-SBA. Furthermore, with its hydrophilic properties, the amine group enhances SBA-15's affinity for water, making GLI-SBA-A more readily soluble. A one-way ANOVA test was conducted, yielding a significance value of 0.000 (p <0.05), which indicates a significant difference in solubility among the data.

Based on the dissolution test results in Figure 7, the percentage of dissolved gliclazide increased compared to pure

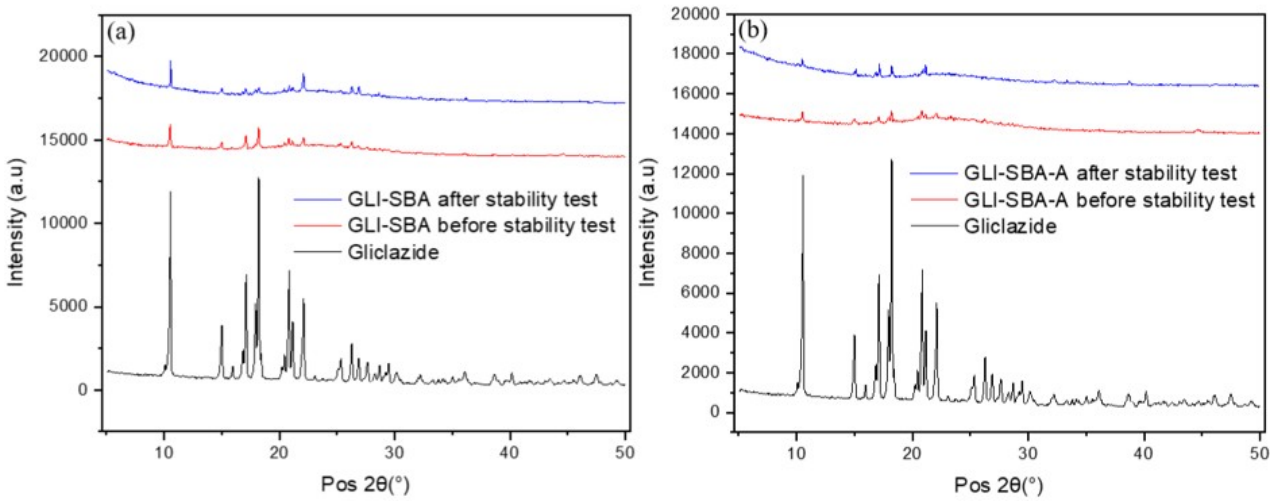

Figure 8. PXRD patterns of Gliclazide, GLI–SBA, GLI–SBA-A, and Their Corresponding Samples After Stability Testing

gliclazide. The difference in the percentage dissolved was significant. Within the first 5 minutes, GLI-SBA dissolved by 45.115% and GLI-SBA-A by 29.069%, whereas pure gliclazide only dissolved by 7.478%. These results were consistent with studies conducted by Adrover et al. (2020), which stated that a sample's solubility and release rate are directly proportional. The dissolution percentage continued to increase in the following minutes until the 570th minute. At the 570th minute, the GLI-SBA sample reached 97.750%, and the GLI-SBA-A sample reached 94.746%, while pure gliclazide only dissolved by 89.161%. Figure 7 also shows that the GLI-SBA sample dissolved more quickly than the GLI-SBA-A sample, indicating that the amine group in SBA-15 mesopores may slow the release rate of gliclazide. The data were analyzed using SPSS, and a one-way ANOVA test was conducted, yielding a significance value of 0.000 (p <0.05), showing that each sample's release rate has a significantly different mean dissolution percentage.

The physical stability of gliclazide in GLI-SBA and GLI-SBA-A was assessed to determine the effects of humidity and temperature on the solid form of the drug (Figure 8). GLI-SBA and GLI-SBA-A largely preserved their amorphous structure throughout the one-month stability test. However, slight peak shifts and increased crystal peak intensity suggest minor transformations in the solid form may have occurred. Nevertheless, the overall diffraction patterns before and after storage show no significant differences, indicating that the samples remained relatively stable. These findings are consistent with those reported by Hasanah et al. (2025), who observed that ticagrelor-SBA-15 retained its amorphous form after one month in a climatic chamber despite some rise in crystalline peak intensity.

4. CONCLUSIONS

Gliclazide adsorbed into the mesopores of SBA-15 showed a 1.375-fold increase in solubility in distilled water compared to pure gliclazide. The solubility of gliclazide adsorbed into the mesopores of SBA-15-A in distilled water increased by 2.334 fold compared to pure gliclazide. However, the functionalization of amine groups on the mesoporous SBA-15 could not control the release profile of gliclazide, as both GLI-SBA and GLI-SBA-A increased the release rate of gliclazide.

5. ACKNOWLEDGMENT

This Research was funded by Universitas Andalas under the Undergraduate Thesis Research Scheme with contract number 271/UN16.19/PT.01.03/PSS/2024.

REFERENCES

Adrover, M. E., M. Pedernera, M. Bonne, B. Lebeau, V. Bucalá, and L. Gallo (2020). Synthesis and Characterization of Mesoporous SBA-15 and SBA-16 as Carriers to Improve Albendazole Dissolution Rate. *Saudi Pharmaceutical Journal*, **28**(1); 15–24

Albayati, T. M., I. K. Salih, and H. F. Alazzawi (2019). Synthesis and Characterization of a Modified Surface of SBA-15 Mesoporous Silica for a Chloramphenicol Drug Delivery System. *Heliyon*, **5**(10); e02539

Banday, M. Z., A. S. Sameer, and S. Nissar (2020). Pathophysiology of Diabetes: An Overview. *Avicenna Journal of Medicine*, **10**(04); 174–188

Bindal, R., D. K. Sharma, and S. K. Chaturvedi (2024). Development and Characterization of Gliclazide Solid Dispersion Using Mixed Solvency Concept. *International Journal of Newgen Research in Pharmacy & Healthcare*; 116–124

Budiman, A., G. Anastasya, A. L. Handini, I. N. Lestari, L. Subra, and D. L. Aulifa (2024). Characterization of Drug with Good Glass-Forming Ability Loaded Mesoporous Silica Nanoparticles and Its Impact Toward In Vitro and In Vivo Studies. *International Journal of Nanomedicine*, **19**; 2199–2225

Dadej, A., A. Woźniak-Braszak, P. Bilski, H. Piotrowska-Kempisty, M. Józkowiak, M. Geszke-Moritz, M. Moritz, D. Dadej, and A. Jelińska (2021). Modification of the Release of Poorly Soluble Sulindac with the APTES-Modified SBA-15 Mesoporous Silica. *Pharmaceutics*, **13**(10); 1693

Domingo-Lopez, D. A., G. Lattanzi, L. H. J. Schreiber, E. J. Wallace, R. Wylie, J. O'Sullivan, E. B. Dolan, and G. P. Duffy (2022). Medical Devices, Smart Drug Delivery, Wearables and Technology for the Treatment of Diabetes Mellitus. *Advanced Drug Delivery Reviews*, **185**; 114280

Estevão, B. M., I. Miletto, N. Hioka, L. Marchese, and E. Gianotti (2021). Mesoporous Silica Nanoparticles Functionalized with Amino Groups for Biomedical Applications. *ChemistryOpen*, **10**(12); 1251–1259

Fitriani, L., H. Azizah, U. Hasanah, and E. Zaini (2023). Enhancement of Curcumin Solubility and Dissolution by Adsorption in Mesoporous SBA-15. *International Journal of Applied Pharmaceutics*, **15**(Special Issue 1); 61–67

Fitriani, L., C. M. Azzahra, A. Jessica, U. Hasanah, and E. Zaini (2024). Improvement of Solubility Usnic Acid Loaded on Mesoporous Silica SBA-15 and Physicochemical Characterization. *Science and Technology Indonesia*, **9**(2); 251–259

Hasanah, U., F. Rizky, M. C. I. M. Amin, and E. Zaini (2025). Ticagrelor Solubility and Dissolution Rate Enhancement Using Mesoporous Silica SBA-15. *Science and Technology Indonesia*, **10**(2); 598–604

Hasanah, U., S. Wikarsa, and S. Asyarie (2021). Various Chloride Salt Addition in Mesoporous Material (SBA-15) Synthesis and Potential as Carrier for Dissolution Enhancer. In *Proceedings of the 6th International Conference on Health Sciences Research*. pages 343–349

He, Y., S. Liang, M. Long, and H. Xu (2017). Mesoporous Silica Nanoparticles as Potential Carriers for Enhanced Drug Solubility of Paclitaxel. *Materials Science and Engineering: C*, **78**; 12–17

Izquierdo-Barba, I., E. Sousa, J. C. Doadrio, A. L. Doadrio, J. P. Pariente, A. Martínez, F. Babonneau, and M. Vallet-Regí (2009). Influence of Mesoporous Structure Type on the Controlled Delivery of Drugs: Release of Ibuprofen from MCM-48, SBA-15 and Functionalized SBA-15. *Journal of Sol-Gel Science and Technology*, **50**(3); 421–429

Knapik-Kowalczuk, J., D. Kramarczyk, K. Chmiel, J. Romanova, K. Kawakami, and M. Paluch (2020). Importance of Mesoporous Silica Particle Size in the Stabilization of Amorphous Pharmaceuticals—The Case of Simvastatin. *Pharmaceutics*, **12**(4); 384

Letchmanan, K., S. C. Shen, W. K. Ng, and R. B. H. Tan (2017). Dissolution and Physicochemical Stability Enhancement of Artemisinin and Mefloquine Co-Formulation via Nano-Confinement with Mesoporous SBA-15. *Colloids and Surfaces B: Biointerfaces*, **155**; 560–568

Liou, T. H., G. W. Chen, and S. Yang (2022). Preparation of Amino-Functionalized Mesoporous SBA-15 Nanoparticles and the Improved Adsorption of Tannic Acid in Wastewater. *Nanomaterials*, **12**(5); 791

Maggi, L., A. Canobbio, G. Bruni, G. Musitelli, and U. Conte (2015). Improvement of the Dissolution Behavior of Gliclazide, a Slightly Soluble Drug, Using Solid Dispersions. *Journal of Drug Delivery Science and Technology*, **26**; 17–23

Maleki, A. and M. Hamidi (2016). Dissolution Enhancement of a Model Poorly Water-Soluble Drug, Atorvastatin, with Ordered Mesoporous Silica: Comparison of MSF with SBA-15 as Drug Carriers. *Expert Opinion on Drug Delivery*, **13**(2); 171–181

Munguía-Cortés, L., I. Pérez-Hermosillo, R. Ojeda-López, J. M. Esparza-Schulz, C. Felipe-Mendoza, A. Cervantes-Uribe, and A. Domínguez-Ortiz (2017). APTES-Functionalization of SBA-15 Using Ethanol or Toluene: Textural Characterization and Sorption Performance of Carbon Dioxide. *Journal of the Mexican Chemical Society*, **61**(4); 273–281

Pevná, V., L. Zauška, A. Benziane, G. Vámosi, V. Girman, M. Miklóšová, V. Zeleňák, V. Huntošová, and M. Almáši (2023). Effective Transport of Aggregated Hypericin Encapsulated in SBA-15 Nanoporous Silica Particles for Photodynamic Therapy of Cancer Cells. *Journal of Photochemistry and Photobiology B: Biology*, **247**; 112785

Rajamma, A. J., S. B. Sateesha, M. K. Narode, V. R. S. S. Prashanth, and A. M. Karthik (2015). Preparation and Crystallographic Analysis of Gliclazide Polymorphs. *Indian Journal of Pharmaceutical Sciences*, **77**(1); 34

Sahin, I., O. Bakiner, T. Demir, R. Sari, and A. Atmaca (2024). Current Position of Gliclazide and Sulfonylureas in the Contemporary Treatment Paradigm for Type 2 Diabetes: A Scoping Review. *Diabetes Therapy*, **15**(8); 1687–1716

Simos, Y. V., K. Spyrou, M. Patila, N. Karouta, H. Stamatis, D. Gournis, E. Dounousi, and D. Peschos (2021). Trends of Nanotechnology in Type 2 Diabetes Mellitus Treatment. *Asian Journal of Pharmaceutical Sciences*, **16**(1); 62–76

Wang, M. and B. Duan (2019). Materials and Their Biomedical Applications. In *Encyclopedia of Biomedical Engineering*, volume 1–3. pages 135–152

Wawrzyńczak, A., I. Nowak, and A. Feliczak-Guzik (2023). SBA-15- and SBA-16-Functionalized Silicas as New Carriers of Niacinamide. *International Journal of Molecular Sciences*, **24**(24); 17567

Weeda, E. R., C. I. Coleman, C. A. McHorney, C. Crivera, J. R. Schein, and D. M. Sobieraj (2016). Impact of Once- or Twice-Daily Dosing Frequency on Adherence to Chronic Cardiovascular Disease Medications: A Meta-Regression Analysis. *International Journal of Cardiology*, **216**; 104–109

Yaghobi, N., L. Hajiaghababaei, A. Badiei, M. R. Ganjali, and G. M. Ziarani (2019). Controlled Release of Amoxicillin from Bis(2-Hydroxyethyl)Amine Functionalized SBA-15 as a Mesoporous Sieve Carrier. *Journal of Chemical Health Risks*, **9**(3); 253

Zhang, W., H. Liu, X. Qiu, F. Zuo, and B. Wang (2024). Mesoporous Silica Nanoparticles as a Drug Delivery Mechanism. *Open Life Sciences*, **19**(1); 20220867

